*International Conference on Mathematics, Computational Methods & Reactor Physics (M&C 2009)*
Saratoga Springs, New York, May 3-7, 2009, on CD-ROM, American Nuclear Society, LaGrange Park, IL (2009)

# Application of the "Functional Monte Carlo" Method to Estimate Continuous Energy $k$-Eigenvalues and Eigenfunctions

**Jinan Yang and Edward W. Larsen**
Department of Nuclear Engineering & Radiological Sciences,
University of Michigan, Ann Arbor, MI, 48109, USA
jinan@umich.edu; edlarsen@umich.edu

## ABSTRACT

In Monte Carlo simulations of $k$-eigenvalue problems, the eigenfunctions are often poorly estimated for optically thick fissile systems with a large dominance ratio, i.e. when the ratio of the second largest to the largest eigenvalue is close to unity. In this case, Monte Carlo estimates of the fission source may never converge unless an extraordinarily large number of particles is used per fission generation. We have proposed a new "functional Monte Carlo" (FMC) method to address this difficulty. The 1-D, monoenergetic FMC results were published in the journal "Nuclear Science and Engineering" in 2008. In the present paper, we extend the FMC method to continuous-energy $k$-eigenvalue problems. The continuous-energy approach has several noticeable differences compared with the monoenergetic approach. In this hybrid FMC method, energy-integrated nonlinear functionals are estimated using standard Monte Carlo techniques with continuous energy. These functionals are then used in an energy-independent low-order equation to estimate the eigenvalue and the energy-integrated flux. The resulting continuous energy FMC estimates of eigenvalue and energy-integrated flux have very small energy truncation errors and statistical errors. However, the FMC method has no spatial or angular truncation errors. Our numerical examples show that the energy-integrated flux converges orders of magnitude faster in the FMC approach than with the standard Monte Carlo approach. The FMC method also produces much more accurate estimates of the eigenvalue.

*Key Words:* "Functional Monte Carlo" method, continuous energy, $k$-eigenvalues, $k$-eigenfunctions

## 1. INTRODUCTION

A principal concern for the Monte Carlo simulation of a $k$-eigenvalue problem is deciding how many inactive cycles are to be skipped, after which the fission source distribution can be safely assumed to have reached equilibrium. For an optically thick system, such an equilibrium distribution is often difficult to achieve because of undersampling of the fission source.

Recently, we introduced a new functional Monte Carlo (FMC) method for $k$-eigenvalue problems which helps to overcome the difficulties that result from undersampling [1, 2]. The FMC method does not employ Monte Carlo techniques to directly estimate the eigenfunction and eigenvalue. Instead, the Monte Carlo method is used to estimate certain nonlinear functionals in a formulation related to the quasi-diffusion (QD) method [3]. These functionals depend only weakly on the eigenfunction. Monte Carlo estimates of the functionals may then be used in the low-order FMC equations to obtain new estimates of the eigenvalue and eigenfunction. In references [1, 2] this method was shown, for monoenergetic problems, to achieve equilibrium using orders of magnitude fewer particles than a conventional Monte Carlo simulation would require.

In the present paper we extend the application of the FMC technique to continuous-energy $k$-eigenvalue problems. This is an important step, because energy-varying cross-sections are much more realistic for practical applications. In the formulation given here, energy-integrated nonlinear functionals are estimated using the standard Monte Carlo method. These functionals are then used in energy-independent, low-order equations to estimate the eigenvalue and the energy-integrated flux. The work presented here rests on two key hypotheses, which we now explicitly state:

*Hypothesis A*: Standard Monte Carlo simulations yield more accurate estimates of the nonlinear functionals than of the energy-integrated flux or $k$-eigenvalue.

*Hypothesis B*: The discrete system of low-order equations containing the nonlinear functionals is not sensitive to small errors in estimated values of the functionals.

We do not attempt to theoretically prove these hypotheses in this paper. However, we do provide strong numerical evidence that both hypotheses are valid. Specifically, we show that, just as was true for $1D$ monoenergetic problems, the FMC method yields much more accurate and rapidly-converged results (than Standard Monte Carlo) for $1D$ continuous-energy problems.

A general presentation of the FMC method for the continuous-energy $k$-eigenvalue problem is summarized in Section 2. In Section 2.1, the application of the FMC method to the continuous energy $k$-eigenvalue problem is formulated in detail. A function $U(x,E)$ is introduced into the equations so as to simplify them by eliminating any dependence on the first-order momentum $\Phi_1(x,E)$. In Section 2.2, results are given for two sample problems, illustrating the remarkable calculational efficiency of the FMC method for the continuous-energy $k$-eigenvalue problem. Conclusions are discussed in Section 3.

## 2. DESCRIPTION OF THE METHOD

We consider a general planar-geometry, continuous energy $k$-eigenvalue problem with vacuum boundaries

$$\mu\frac{\partial\psi}{\partial x}(x,\mu,E)+\Sigma_t(x,E)\psi(x,\mu,E)=\int\int\Sigma_s(x,\mu,\mu',E'\rightarrow E)\psi(x,\mu',E')d\mu'dE'$$
$$+\frac{\chi(x,E)}{2k}\int\int\nu\Sigma_f(x,E')\psi(x,\mu',E')d\mu'dE',\qquad 0<x<X\ , \tag{1a}$$

$$\psi(0,\mu,E)=0\qquad,\qquad 0<\mu\leq 1\ , \tag{1b}$$

$$\psi(X,\mu,E)=0\qquad,\qquad -1\leq\mu<0\ , \tag{1c}$$

with elastic neutron scattering:

$$\Sigma_s(x,\mu,\mu',E'\rightarrow E)=\sum_{n=0}^{\infty}\frac{2n+1}{2}\Sigma_{sn}(x,E'\rightarrow E)P_n(\mu)P_n(\mu')\ , \tag{1d}$$

$$\int_0^{\infty}\chi(x,E)dE=1\ , \tag{1e}$$

where

$$\begin{aligned}
\Sigma_{sn}(x, E' \to E) &= 2\pi \int_{-1}^{1} P_n(\mu_0)\Sigma_s(x, \mu_0, E' \to E)d\mu_0 \\
&= 2\pi \int_{-1}^{1} P_n(\mu_0)\Sigma_s(x, E')P(E' \to E)\frac{\delta(\mu_0 - \hat{\mu}_0)}{2\pi}d\mu_0 \\
&= \Sigma_s(x, E')P(E' \to E)P_n(\hat{\mu}_0) \ , \\
\hat{\mu_0}(E' \to E) &= \left(\frac{A+1}{2}\right)\sqrt{\frac{E}{E'}} - \left(\frac{A-1}{2}\right)\sqrt{\frac{E'}{E}} \ , \\
P(E' \to E) &= \begin{cases} \frac{1}{(1-\alpha)E'} & \alpha E' < E < E' \\ 0 & \text{otherwise} \end{cases} .
\end{aligned}$$

Our procedure to solve Eqs. (1) follows closely the three-step procedure used earlier to solve the monoenergetic low-order FMC equations [2]. Importantly, we shall introduce a function $U(x, E)$ into these equations to accommodate the continuous-energy feature. Our procedure is given below.

### 2.1. General FMC Procedure to Solve Continuous-Energy $k$-Eigenvalue Problems

The FMC equations are obtained by calculating certain space-angle moments of Eqs. (1). Following the first step from reference [2], we begin by operating on Eq. (1a) with $\int_{-1}^{1} \mu^n(\cdot)\, d\mu$ for $n = 0$ and 1. We define

$$\Phi_n(x, E) = \int_{-1}^{1} \mu^n \psi(x, \mu, E)d\mu \ , \qquad n = 0, 1, 2 \ . \tag{2}$$

For $n = 0$, one finds

$$\begin{aligned}
&\frac{\partial}{\partial x}\Phi_1(x, E) + \Sigma_t(x, E)\Phi_0(x, E) \\
&\quad = \int_0^\infty \Sigma_{s0}(x, E' \to E)\Phi_0(x, E')dE' + \frac{\chi(x, E)}{k}\int_0^\infty \nu\Sigma_f(x, E')\Phi_0(x, E')dE' \ ; \quad (3)
\end{aligned}$$

and for $n = 1$, we have

$$\frac{\partial}{\partial x}\Phi_2(x, E) + \Sigma_t(x, E)\Phi_1(x, E) = \int_0^\infty \Sigma_{s1}(x, E' \to E)\Phi_1(x, E')dE' \ . \tag{4}$$

Next, we subtract a term $u(x, E)\Phi_1(x, E)$ from both side of Eq. (4). [The definition of $u(x, E)$ is stated below. ]

$$\begin{aligned}
&\frac{\partial}{\partial x}\Phi_2(x, E) + [\Sigma_t(x, E) - u(x, E)]\Phi_1(x, E) \\
&\qquad = \int_0^\infty \Sigma_{s1}(x, E' \to E)\Phi_1(x, E')dE' - u(x, E)\Phi_1(x, E) \ .
\end{aligned}$$

Rearranging, we get

$$\Phi_1(x,E) = -\frac{1}{\Sigma_t(x,E)-u(x,E)}\frac{\partial}{\partial x}\Phi_2(x,E) + \frac{1}{\Sigma_t(x,E)-u(x,E)}\left[\int_0^\infty \Sigma_{s1}(x,E'\to E)\Phi_1(x,E')dE' - u(x,E)\Phi_1(x,E)\right]. \tag{5}$$

Now we calculate the energy integrals in Eqs. (3) and (5). Defining

$$\phi_n(x) = \int_0^\infty \Phi_n(x,E)dE\ , \quad n=0,1\ ,$$

and operating on Eq. (3) by $\int_0^\infty(\cdot)dE$, we get:

$$\frac{d}{dx}\phi_1(x) + \int_0^\infty \Sigma_t(x,E)\Phi_0(x,E)dE = \int_0^\infty \Sigma_s(x,E')\Phi_0(x,E')dE' + \frac{1}{k}\int_0^\infty \nu\Sigma_f(x,E')\Phi_0(x,E')dE'\ . \tag{6}$$

However,

$$\begin{aligned}\Sigma_t(x,E) &= \Sigma_s(x,E)+\Sigma_\gamma(x,E)+\Sigma_f(x,E)\\ &= \Sigma_s(x,E)+\Sigma_a(x,E)\ .\end{aligned} \tag{7}$$

Then Eq. (6) becomes

$$\frac{d}{dx}\phi_1(x) + \int_0^\infty \Sigma_a(x,E)\Phi_0(x,E)dE = \frac{1}{k}\int_0^\infty \nu\Sigma_f(x,E)\Phi_0(x,E)dE\ . \tag{8}$$

Also, operating on Eq. (5) by $\int_0^\infty(\cdot)dE$, we get

$$\phi_1(x) = -\int_0^\infty \frac{1}{\Sigma_t(x,E)-u(x,E)}\frac{\partial}{\partial x}\Phi_2(x,E)dE + \int_0^\infty \frac{1}{\Sigma_t(x,E)-u(x,E)} \times\left[\int_0^\infty \Sigma_{s1}(x,E'\to E)\Phi_1(x,E')dE' - u(x,E)\Phi_1(x,E)\right]dE\ .$$

Exchanging the dummy variables $E$ and $E'$, we find

$$\phi_1(x) = -\int_0^\infty \frac{1}{\Sigma_t(x,E)-u(x,E)}\frac{\partial}{\partial x}\Phi_2(x,E)dE + \int_0^\infty \underbrace{\left[\int_0^\infty \frac{\Sigma_{s1}(x,E\to E')}{\Sigma_t(x,E')-u(x,E')}dE' - \frac{u(x,E)}{\Sigma_t(x,E)-u(x,E)}\right]}_{\text{(Set this term = 0.)}}\Phi_1(x,E)dE\ .$$

Now we require that $u(x,E)$ be chosen to eliminate the $\Phi_1(x,E)$ term, yielding

$$\int_0^\infty \frac{\Sigma_{s1}(x,E\rightarrow E')}{\Sigma_t(x,E')-u(x,E')}dE' - \frac{u(x,E)}{\Sigma_t(x,E)-u(x,E)} = 0\ ;$$

or:

$$\frac{\Sigma_t(x,E)}{\Sigma_t(x,E)-u(x,E)} - 1 = \int_0^\infty \frac{\Sigma_{s1}(x,E\rightarrow E')}{\Sigma_t(x,E')-u(x,E')}dE'. \tag{9}$$

Defining

$$U(x,E) = \frac{1}{\Sigma_t(x,E)-u(x,E)}\ ,$$

then Eq. (9) can be rewritten as the linear equation

$$\Sigma_t(x,E)U(x,E) - \int_0^\infty \Sigma_{s1}(x,E\rightarrow E')U(x,E')dE' = 1\ . \tag{10}$$

Henceforth, we assume that $U(x,E)$ is the solution of Eq. (10). [Note that if scattering is isotropic, then $U(x,E)=\Sigma_t^{-1}(x,E)$ .] Then the equation for $\phi_1(x)$ becomes

$$\phi_1(x) = -\int_0^\infty U(x,E)\frac{\partial}{\partial x}\Phi_2(x,E)dE\ . \tag{11}$$

Substituting Eq. (11) for $\phi_1(x)$ into Eq. (8) then gives:

$$\begin{aligned} -\frac{\partial}{\partial x}\int_0^\infty U(x,E)\frac{\partial}{\partial x}\Phi_2(x,E)dE + \int_0^\infty \Sigma_a(x,E)\Phi_0(x,E)dE \\ = \frac{1}{k}\int_0^\infty \nu\Sigma_f(x,E)\Phi_0(x,E)dE\ . \end{aligned} \tag{12}$$

Eq. (12) completes the first step from [2].

In the next step, we perform the spatial integrations using the same *tent functions* $f(x)$ as were used for monoenergetic problems. We define a spatial grid $0 = x_{1/2} < x_{3/2} < \cdots < x_{J+1/2} = X$, and for each grid point $x_{j+1/2}$ the *tent functions* $f(x)$ are

$$f(x) = f_{1/2} = \begin{cases} \frac{1}{h_1}(x_{3/2}-x) & ,\ 0 = x_{1/2} < x < x_{3/2} \\ 0 & ,\ \text{otherwise}\ , \end{cases} \tag{13a}$$

for $1 \le j \le J-1$,

$$f(x) = f_{j+1/2} = \begin{cases} \frac{1}{h_j}(x-x_{j-1/2}) & ,\ x_{j-1/2} < x < x_{j+1/2} \\ \frac{1}{h_{j+1}}(x_{j+3/2}-x) & ,\ x_{j+1/2} < x < x_{j+3/2} \\ 0 & ,\ \text{otherwise}\ , \end{cases} \tag{13b}$$

and for $j = J$,

$$f(x) = f_{J+1/2} = \begin{cases} \frac{1}{h_J}(x-x_{J-1/2}) & ,\ x_{J-1/2} < x < x_{J+1/2} = X \\ 0 & ,\ \text{otherwise}\ . \end{cases} \tag{13c}$$

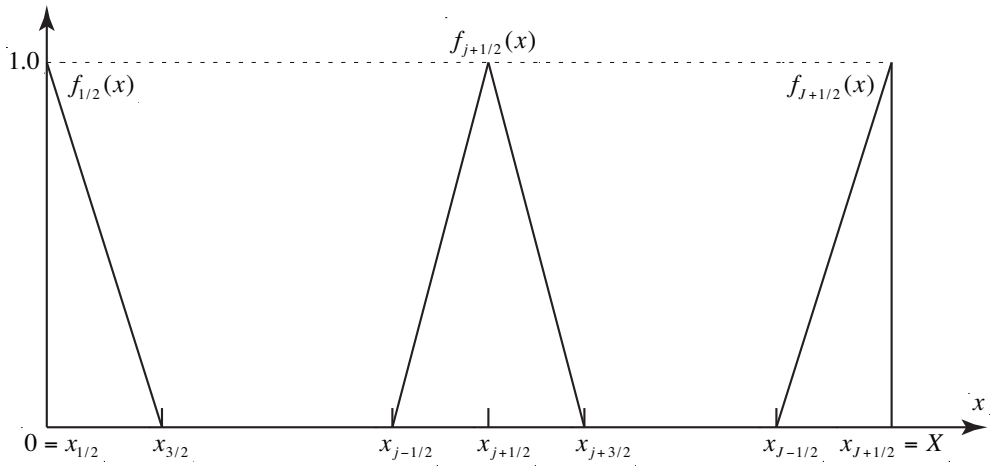


**Figure 1. The Tent Functions**

For each $j$, we now perform the operation $\int_0^X f_{j+1/2}(x)(\cdot)dx$ on Eq. (12). For $j = 0$ we obtain

$$
\begin{aligned}
-\int_{x_{1/2}}^{x_{3/2}} f_{1/2}(x)\frac{\partial}{\partial x}\int_0^\infty U(x,E)\frac{\partial}{\partial x}\Phi_2(x,E)dEdx \\
+\int_{x_{1/2}}^{x_{3/2}} f_{1/2}(x)\int_0^\infty \Sigma_a(x,E)\Phi_0(x,E)dEdx \\
=\frac{1}{k}\int_{x_{1/2}}^{x_{3/2}} f_{1/2}(x)\int_0^\infty \nu\Sigma_f(x,E)\Phi_0(x,E)dEdx\ . \qquad (14)
\end{aligned}
$$

Integrating the first term by parts gives

$$
\begin{aligned}
&-\int_{x_{1/2}}^{x_{3/2}} f_{1/2}(x)\frac{\partial}{\partial x}\int_0^\infty U(x,E)\frac{\partial}{\partial x}\Phi_2(x,E)dE\,dx \\
&=-f_{1/2}(x)\int_0^\infty U(x,E)\frac{\partial}{\partial x}\Phi_2(x,E)dE|_{x_{1/2}}^{x_{3/2}}-\frac{1}{h_1}\int_{x_{1/2}}^{x_{3/2}}\int_0^\infty U(x,E)\frac{\partial}{\partial x}\Phi_2(x,E)dE \\
&=\int_0^\infty U(x_{1/2},E)\frac{\partial}{\partial x}\Phi_2(x_{1/2},E)dE-\frac{1}{h_1}\int_{x_{1/2}}^{x_{3/2}}\int_0^\infty U(x,E)\frac{\partial}{\partial x}\Phi_2(x,E)dE \\
&\quad=-\phi_1(x_{1/2})-\frac{1}{h_1}\int_0^\infty U_1(E)[\Phi_2(x_{3/2},E)-\Phi_2(x_{1/2},E)]dE\ . \qquad (15)
\end{aligned}
$$

Here we have assumed that each spatial cell $[x_{j-1/2}, x_{j+1/2}]$ consists of a single material. Therefore in the $j^{th}$ cell, $U(x,E) = U_j(E)$ independent of $x$.

From the vacuum boundary condition, we have

$$\phi_1(x_{1/2}) = \int_0^\infty \int_{-1}^1 \mu\psi(0,\mu,E)d\mu dE$$

$$
\begin{aligned}
&= \int_0^\infty \left[ \int_0^1 \mu\psi(0,\mu,E)d\mu + \int_{-1}^0 \mu\psi(0,\mu,E)d\mu \right] dE \\
&= \int_0^\infty \int_{-1}^0 \mu\psi(0,\mu,E)d\mu dE \\
&= -\int_0^\infty \int_{-1}^0 |\mu|\psi(0,\mu,E)d\mu dE \ . \qquad (16)
\end{aligned}
$$

Substituting Eq. (16) into Eq. (15), the first term in Eq. (14) can be written

$$
\begin{aligned}
&-\int_{x_{1/2}}^{x_{3/2}} f_{1/2}(x)\frac{\partial}{\partial x}\int_0^\infty U(x,E)\frac{\partial}{\partial x}\Phi_2(x,E)dE\ dx \\
&= \int_0^\infty \int_{-1}^0 |\mu|\psi(0,\mu,E)d\mu dE - \frac{1}{h_1}\int_0^\infty U_1(E)[\Phi_2(x_{3/2},E) - \Phi_2(x_{1/2},E)]dE \ . \qquad (17)
\end{aligned}
$$

Thus, for $j = 0$, Eq. (14) becomes

$$
\begin{aligned}
\int_0^\infty \int_{-1}^0 |\mu|\psi(0,\mu,E)d\mu dE - \frac{1}{h_1}\int_0^\infty U_1(E)[\Phi_2(x_{3/2},E) - \Phi_2(x_{1/2},E)]dE& \\
+ \int_{x_{1/2}}^{x_{3/2}} f_{1/2}(x)\int_0^\infty \Sigma_a(x,E)\Phi_0(x,E)dEdx& \\
= \frac{1}{k}\int_{x_{1/2}}^{x_{3/2}} f_{1/2}(x)\int_0^\infty \nu\Sigma_f(x,E)\Phi_0(x,E)dEdx \ . \qquad (18)&
\end{aligned}
$$

We emphasize that this equation is exact; no approximations were introduced to derive it.

For the interior $j$'s, i.e. for $1 \le j \le J-1$, we find

$$
\begin{aligned}
-\int_{x_{j-1/2}}^{x_{j+3/2}} f_{j+1/2}(x)\frac{\partial}{\partial x}\int_0^\infty U(x,E)\frac{\partial}{\partial x}\Phi_2(x,E)dEdx& \\
+ \int_{x_{j-1/2}}^{x_{j+3/2}} f_{j+1/2}(x)\int_0^\infty \Sigma_a(x,E)\Phi_0(x,E)dEdx& \\
= \frac{1}{k}\int_{x_{j-1/2}}^{x_{j+3/2}} f_{j+1/2}(x)\int_0^\infty \nu\Sigma_f(x,E)\Phi_0(x,E)dEdx \ . \qquad (19)&
\end{aligned}
$$

Integrating the first term of Eq. (19) by parts, we get

$$
\begin{aligned}
&-\int_{x_{j-1/2}}^{x_{j+3/2}} f_{j+1/2}(x)\left[\frac{\partial}{\partial x}\int_0^\infty U(x,E)\frac{\partial}{\partial x}\Phi_2(x,E)dE\right]dx \\
&\quad = \int_{x_{j-1/2}}^{x_{j+3/2}} \frac{d}{dx}f_{j+1/2}(x)\left[\int_0^\infty U(x,E)\frac{\partial}{\partial x}\Phi_2(x,E)dE\right]dx \\
&\quad = \int_{x_{j-1/2}}^{x_{j+1/2}} \frac{1}{h_j}\left[\int_0^\infty U(x,E)\frac{\partial}{\partial x}\Phi_2(x,E)dE\right]dx
\end{aligned}
$$

$$
\begin{aligned}
&- \int_{x_{j+1/2}}^{x_{j+3/2}} \frac{1}{h_{j+1}} \left[ \int_0^\infty U(x,E) \frac{\partial}{\partial x} \Phi_2(x,E) dE \right] dx \\
&= \frac{1}{h_j} \int_0^\infty U_j(E) \left[ \Phi_2(x_{j+1/2},E) - \Phi_2(x_{j-1/2},E) \right] dE \\
&\quad - \frac{1}{h_{j+1}} \int_0^\infty U_{j+1}(E) \left[ \Phi_2(x_{j+3/2},E) - \Phi_2(x_{j+1/2},E) \right] dE \ . \qquad (20)
\end{aligned}
$$

Substituting Eq. (20) into Eq. (19) then leads to

$$
\begin{aligned}
&\frac{1}{h_j} \int_0^\infty U_j(E) \left[ \Phi_2(x_{j+1/2},E) - \Phi_2(x_{j-1/2},E) \right] dE \\
&\quad - \frac{1}{h_{j+1}} \int_0^\infty U_{j+1}(E) \left[ \Phi_2(x_{j+3/2},E) - \Phi_2(x_{j+1/2},E) \right] dE \\
&\quad + \int_{x_{j-1/2}}^{x_{j+3/2}} f_{j+1/2}(x) \int_0^\infty \Sigma_a(x,E) \Phi_0(x,E) dE dx \\
&\quad = \frac{1}{k} \int_{x_{j-1/2}}^{x_{j+3/2}} f_{j+1/2}(x) \int_0^\infty \nu \Sigma_f(x,E) \Phi_0(x,E) dE dx \ . \qquad (21)
\end{aligned}
$$

These equations also are exact.

For $j = J$, following similar steps as for $j = 0$, we obtain another exact equation:

$$
\begin{aligned}
&\int_0^\infty \int_0^1 \mu \psi(x_{J+1/2},\mu,E) d\mu dE + \frac{1}{h_J} \int_0^\infty U_J(E) [\Phi_2(x_{J+1/2},E) - \Phi_2(x_{J-1/2},E)] dE \\
&\qquad + \int_{x_{J-1/2}}^{x_{J+1/2}} f_{J+1/2}(x) \int_0^\infty \Sigma_a(x,E) \Phi_0(x,E) dE dx \\
&\qquad = \frac{1}{k} \int_{x_{J-1/2}}^{x_{J+1/2}} f_{J+1/2}(x) \int_0^\infty \nu \Sigma_f(x,E) \Phi_0(x,E) dE dx \ . \qquad (22)
\end{aligned}
$$

We have now obtained a system of $J+1$ discrete equations, Eqs. (18), (21) and (22), which are exactly satisfied by the solution $\psi(x,\mu,E)$ and $k$ of Eqs. (1). This completes the second step in [2].

In the third step, we use Eqs. (18), (21) and (22) to define energy-integrated nonlinear functionals. These functionals are then used in energy-independent low-order equations derived from Eqs. (18), (21) and (22) to estimate the eigenvalue and the energy-integrated flux.

We first define volume-averaged fluxes as in [2]:

$$
\bar{\phi}(x_{j+1/2}) = \int_{x_{j-1/2}}^{x_{j+3/2}} g_{j+1/2}(x) \phi_0(x) \, dx \ , \qquad (23)
$$

where $x_j = (x_{j+1/2} + x_{j-1/2})/2$ = midpoint of the $j^{th}$ cell , and $g_{j+1/2}(x)$ are defined as: for $j = 0$:

$$
g_{1/2}(x) = \begin{cases} \frac{2}{h_1} & , \quad x_{1/2} \le x \le x_1 \\ 0 & , \quad \text{otherwise} \ , \end{cases} \qquad (24a)
$$

for $1 \leq j \leq J-1$:

$$g_{j+1/2}(x) = \begin{cases} \frac{2}{h_j + h_{j+1}} & , \quad x_j \leq x \leq x_{j+1} \\ 0 & , \quad \text{otherwise} \ , \end{cases} \tag{24b}$$

and for $j = J$:

$$g_{J+1/2}(x) = \begin{cases} \frac{2}{h_J} & , \quad x_J \leq x \leq x_{J+1/2} \\ 0 & , \quad \text{otherwise} \ . \end{cases} \tag{24c}$$

Next, we multiply and divide each term in Eqs. (18), (21), and (22) by a suitable volume-averaged flux defined by Eq. (23). This gives the following equivalent set of $J+1$ equations:

$$\begin{aligned} &\left[ \left( \frac{\int_0^\infty \int_{-1}^0 |\mu| \psi(0,\mu,E) d\mu dE}{\int_0^\infty \int_{x_{1/2}}^{x_{3/2}} g_{1/2}(x) \Phi_0(x,E) dx dE} \right) + \left( \frac{\int_{x_{1/2}}^{x_{3/2}} f_{1/2}(x) \int_0^\infty \Sigma_a(x,E) \Phi_0(x,E) dE dx}{\int_0^\infty \int_{x_{1/2}}^{x_{3/2}} g_{1/2}(x) \Phi_0(x,E) dx dE} \right) \right. \\ &\quad \left. + \frac{1}{h_1} \left( \frac{\int_0^\infty U_1(E) \Phi_2(x_{1/2},E) dE}{\int_0^\infty \int_{x_{1/2}}^{x_{3/2}} g_{1/2}(x) \Phi_0(x,E) dx dE} \right) \right] \bar{\phi}(x_{1/2}) \\ &\quad - \frac{1}{h_1} \left( \frac{\int_0^\infty U_1(E) \Phi_2(x_{3/2},E) dE}{\int_0^\infty \int_{x_{1/2}}^{x_{5/2}} g_{3/2}(x) \Phi_0(x,E) dx dE} \right) \bar{\phi}(x_{3/2}) \\ &\quad = \frac{1}{k} \left( \frac{\int_{x_{1/2}}^{x_{3/2}} f_{1/2}(x) \int_0^\infty \nu\Sigma_f(x,E) \Phi_0(x,E) dE dx}{\int_0^\infty \int_{x_{1/2}}^{x_{3/2}} g_{1/2}(x) \Phi_0(x,E) dx dE} \right) \bar{\phi}(x_{1/2}) \ , \end{aligned} \tag{25a}$$

$$\begin{aligned} &- \frac{1}{h_j} \left( \frac{\int_0^\infty U_j(E) \Phi_2(x_{j-1/2},E) dE}{\int_0^\infty \int_{x_{j-3/2}}^{x_{j+1/2}} g_{j-1/2}(x) \Phi_0(x,E) dx \ dE} \right) \bar{\phi}(x_{j-1/2}) \\ &+ \left[ \frac{1}{h_j} \left( \frac{\int_0^\infty U_j(E) \Phi_2(x_{j+1/2},E) dE}{\int_0^\infty \int_{x_{j-1/2}}^{x_{j+3/2}} g_{j+1/2}(x) \Phi_0(x,E) dx \ dE} \right) + \frac{1}{h_{j+1}} \left( \frac{\int_0^\infty U_{j+1}(E) \Phi_2(x_{j+1/2},E) dE}{\int_0^\infty \int_{x_{j-1/2}}^{x_{j+3/2}} g_{j+1/2} \Phi_0(x,E) dx \ dE} \right) \right. \\ &\quad \left. + \left( \frac{\int_{x_{j-1/2}}^{x_{j+3/2}} f_{j+1/2}(x) \int_0^\infty \Sigma_a(x,E) \Phi_0(x,E) dx \ dE}{\int_0^\infty \int_{x_{j-1/2}}^{x_{j+3/2}} g_{j+1/2}(x) \Phi_0(x,E) dx \ dE} \right) \right] \bar{\phi}(x_{j+1/2}) \\ &\quad - \frac{1}{h_{j+1}} \left( \frac{\int_0^\infty U_{j+1}(E) \Phi_2(x_{j+3/2},E) dE}{\int_0^\infty \int_{x_{j+1/2}}^{x_{j+5/2}} g_{j+3/2} \Phi_0(x,E) dx \ dE} \right) \bar{\phi}(x_{j+3/2}) \\ &= \frac{1}{k} \left( \frac{\int_{x_{j-1/2}}^{x_{j+3/2}} f_{j+1/2}(x) \int_0^\infty \nu\Sigma_f(x,E) \Phi_0(x,E) dx \ dE}{\int_0^\infty \int_{x_{j-1/2}}^{x_{j+3/2}} g_{j+1/2}(x) \Phi_0(x,E) dx \ dE} \right) \bar{\phi}(x_{j+1/2}), \quad 1 \leq j \leq J-1 \ , \end{aligned} \tag{25b}$$

and:

$$- \frac{1}{h_J} \left( \frac{\int_0^\infty U_J(E) \Phi_2(x_{J-1/2},E) dE}{\int_0^\infty \int_{x_{J-3/2}}^{x_{J+1/2}} g_{J-1/2}(x) \Phi_0(x,E) dx dE} \right) \bar{\phi}(x_{J-1/2})$$

$$\left[\left(\frac{\int_0^\infty\int_0^1 \mu\psi(x_{J+1/2},\mu,E)d\mu dE}{\int_0^\infty\int_{x_{J-1/2}}^{x_{J+1/2}} g_{J+1/2}(x)\Phi_0(x,E)dxdE}\right)+\left(\frac{\int_{x_{J-1/2}}^{x_{J+1/2}} f_{J+1/2}(x)\int_0^\infty \Sigma_a(x,E)\Phi_0(x,E)dEdx}{\int_0^\infty\int_{x_{J-1/2}}^{x_{J+1/2}} g_{J+1/2}(x)\Phi_0(x,E)dxdE}\right)\right.$$
$$\left.+\frac{1}{h_J}\left(\frac{\int_0^\infty U_J(E)\Phi_2(x_{J+1/2},E)dE}{\int_0^\infty\int_{x_{J-1/2}}^{x_{J+1/2}} g_{J+1/2}(x)\Phi_0(x,E)dxdE}\right)\right]\bar{\phi}_(x_{J+1/2})$$
$$=\frac{1}{k}\left(\frac{\int_{x_{J-1/2}}^{x_{J+1/2}} f_{J+1/2}(x)\int_0^\infty \nu\Sigma_f(x,E)\Phi_0(x,E)dEdx}{\int_0^\infty\int_{x_{J-1/2}}^{x_{J+1/2}} g_{J+1/2}(x)\Phi_0(x,E)dxdE}\right)\bar{\phi}_(x_{J+1/2})\ . \tag{25c}$$

We rewrite Eqs. (25) by defining the following energy, angular, and spatially-integrated nonlinear functionals:

$$B_{1/2}=\frac{\int_0^\infty\int_{-1}^0 |\mu|\psi(0,\mu,E)d\mu dE}{\int_0^\infty\int_{x_{1/2}}^{x_{3/2}} g_{1/2}(x)\Phi_0(x,E)dxdE}\ , \tag{26a}$$

$$B_{J+1/2}=\frac{\int_0^\infty\int_0^1 \mu\psi(x_{J+1/2},\mu,E)d\mu dE}{\int_0^\infty\int_{x_{J-1/2}}^{x_{J+1/2}} g_{J+1/2}(x)\Phi_0(x,E)dxdE}\ , \tag{26b}$$

$$F_{j+1/2}=\frac{\int_{x_{j-1/2}}^{x_{j+3/2}} f_{j+1/2}(x)\int_0^\infty \nu\Sigma_f(x,E)\Phi_0(x,E)dE\ dx}{\int_0^\infty\int_{x_{j-1/2}}^{x_{j+3/2}} g_{j+1/2}(x)\Phi_0(x,E)dx\ dE}\ , \tag{26c}$$

$$A_{j+1/2}=\frac{\int_{x_{j-1/2}}^{x_{j+3/2}} f_{j+1/2}(x)\int_0^\infty \Sigma_a(x,E)\Phi_0(x,E)dx\ dE}{\int_0^\infty\int_{x_{j-1/2}}^{x_{j+3/2}} g_{j+1/2}(x)\Phi_0(x,E)dE\ dx}\ , \tag{26d}$$

$$U^L_{j+1/2}=\frac{\int_0^\infty U_{j+1}(E)\Phi_2(x_{j+1/2},E)dE}{\int_0^\infty\int_{x_{j-1/2}}^{x_{j+3/2}} g_{j+1/2}(x)\Phi_0(x,E)dx\ dE}\ , \tag{26e}$$

$$U^R_{j+1/2}=\frac{\int_0^\infty U_j(E)\Phi_2(x_{j+1/2},E)dE}{\int_0^\infty\int_{x_{j-1/2}}^{x_{j+3/2}} g_{j+1/2}(x)\Phi_0(x,E)dx\ dE}\ . \tag{26f}$$

With these definitions, Eqs. (25) may be written:

$$\left[B_{1/2}+A_{1/2}+\frac{1}{h_1}U^L_{1/2}\right]\bar{\phi}(x_{1/2})-\frac{1}{h_1}U^R_{3/2}\bar{\phi}(x_{3/2})=\frac{1}{k}F_{1/2}\bar{\phi}(x_{1/2})\ , \tag{27a}$$

$$-\frac{1}{h_j}U^L_{j-1/2}\bar{\phi}(x_{j-1/2})+\left[\frac{1}{h_j}U^R_{j+1/2}+\frac{1}{h_{j+1}}U^L_{j+1/2}+A_{j+1/2}\right]\bar{\phi}(x_{j+1/2})$$
$$-\frac{1}{h_{j+1}}U^R_{j+3/2}\bar{\phi}(x_{j+3/2})=\frac{1}{k}F_{j+1/2}\bar{\phi}(x_{j+1/2}),\quad 1\le j\le J-1\ , \tag{27b}$$

$$-\frac{1}{h_J}U^L_{J-1/2}\bar{\phi}(x_{J-1/2})+\left[B_{J+1/2}+A_{J+1/2}+\frac{1}{h_J}U^R_{J+1/2}\right]\bar{\phi}(x_{J+1/2})=\frac{1}{k}F_{J+1/2}\bar{\phi}(x_{J+1/2})\ . \tag{27c}$$

This discrete system of equations has the basic form of a spatially-discretized 1-D monoenergetic diffusion $k$-eigenvalue problem.

The integrals in each of the functionals defined in Eqs. (26) can be evaluated using standard Monte Carlo methods. Because each functional is a ratio of two integrals, the estimated values of the functionals should have smaller statistical errors than the estimated values of the integrals themselves.

Once the estimates of the functionals are obtained, Eqs. (25) then become an algebraic system of $J+1$ energy-independent, low-order equations, which can easily be solved to estimate the $k$-eigenvalue and the energy-integrated volume-averaged scalar fluxes $\bar{\phi}_{j+1/2}$. If the estimated values of the nonlinear functionals are exact, then the resulting values of $k$ and $\bar{\phi}_{j+1/2}$ will also be exact. Thus, even though the FMC contains a "low-order" problem which is solved on a grid, the method contains no spatial truncation errors. The only errors are statistical, due to the Monte Carlo-estimated values of the functionals.

We also note that the resulting values of $\bar{\phi}(x_{j+1/2})$ can be used to derive an updated estimate of the fission source. From Eqs. (26c) and (23),

$$F_{j+1/2}\bar{\phi}(x_{j+1/2}) = \left[\frac{\int_{x_{j-1/2}}^{x_{j+3/2}} f_{j+1/2}(x)\int_0^\infty \nu\Sigma_f(x,E)\Phi_0(x,E)dE\,dx}{\int_{x_{j-1/2}}^{x_{j+3/2}}\int_0^\infty g_{j+1/2}(x)\Phi_0(x,E)dE\,dx}\right] \times \left[\int_{x_{j-1/2}}^{x_{j+3/2}} g_{j+1/2}(x)\int_0^\infty \Phi_0(x,E)dE\,dx\right] ,$$

so this product yields an updated estimate of:

$$\hat{F}_{j+1/2} = \int_{x_{j-1/2}}^{x_{j+3/2}} f_{j+1/2}(x)\int_0^\infty \nu\Sigma_f(x,E)\Phi_0(x,E)dE\,dx .$$

This result could be used to construct a more accurate fission source for the next cycle, but we did not do this in the calculations presented in this paper.

Finally, we summarize the procedures used in this paper to apply the FMC method to the continuous energy problem defined by Eqs. (1):

1. First, we determine an accurate solution $U(x,E)$ of Eq. (10). This is a simple energy-dependent problem that only needs to be solved once for each material region in the problem. For brevity, we do not discuss here the specific method that we used in our simulations. This calculation can be done in many ways and is not a significant complication.
2. Next, we run a standard Monte Carlo simulation of Eqs. (1). The resulting standard Monte Carlo estimate of $k$ is obtained by averaging the $k$ for each cycle over all active cycles. We also tally standard Monte Carlo estimates of the energy-integrated flux by integrating the eigenfunction over angle and energy.
3. During this standard Monte Carlo run, we also estimate the integrals used in Eqs. (26) for each cycle. At the end of each active cycle, the estimated values of the integrals are used to estimate the functionals $F(x_{j+1/2})$, $A(x_{j+1/2})$, $U^L(x_{j+1/2})$, $U^R(x_{j+1/2})$, $B(x_{1/2})$, and $B(x_{J+1/2})$. These values are introduced into the low-order Eqs. (27), which are then solved to obtain estimates of $k$ and the energy-integrated flux. The FMC estimate of $k$ is obtained by averaging the $k$ values from Eqs. (27) for each cycle over all active cycles.

## 2.2. Numerical Results

Here we apply the FMC method as described above to two continuous-energy $k$-eigenvalue problems. In the first problem, we consider a homogeneous fissile slab of thickness $X = 300$ cm surrounded by $5.0$ cm reflectors. In the second problem, we consider two slightly different fissile regions of thickness $X = 10$ cm separated by a moderator of thickness $24$ cm and surrounded by $5.0$ cm reflectors.

For both problems, fission neutrons are born uniformly within the energy range 13.5 MeV - 14.0 MeV. The Monte Carlo simulation starts with a flat fission source. The fissile slab material consists of $^{56}Fe$ metal, while the reflector and moderator are both $^{27}Al$. The relevant cross sections in both problems have the same format, given by:

$$\Sigma_s(x,E) = \Sigma_{s0}(x) + \Sigma_{s1}(x)\sqrt{\frac{E_0}{E}}\ , \tag{28a}$$

$$\Sigma_\gamma(x,E) = \Sigma_\gamma(x)\sqrt{\frac{E_0}{E}}\ , \tag{28b}$$

$$\Sigma_f(x,E) = \Sigma_f(x)\sqrt{\frac{E_0}{E}}\ . \tag{28c}$$

The coefficients in Eqs. (28) are given with the numerical results below.

### 2.2.1. Numerical results for a homogeneous fissile slab with reflectors

The coefficients from Eqs. (28) used for this case are presented in Table I, where $x$ is in units of cm and $\Sigma$ in units of cm$^{-1}$.

**Table I. Cross Section Coefficients for a Homogeneous Fissile Slab Problem**

| Region | Location | $\Sigma_{s0}(x)$ | $\Sigma_{s1}(x)$ | $\Sigma_\gamma(x)$ | $\Sigma_f(x)$ |
|---|---|---|---|---|---|
| 1 | $0 < x < 5$ | 0.856 | 0.01 | 0.01 | 0 |
| 2 | $5 < x < 305$ | 0.856 | 0.01 | 0.01 | 0.0071 |
| 3 | $305 < x < 310$ | 0.856 | 0.01 | 0.01 | 0 |

This problem was run for 1000 cycles, using 50,000 histories/cycle. The FMC calculation employed a grid with $h = 1.0$ cm. We compare results for the estimated energy-integrated flux, averaged over 100 cycle intervals (from a 1000-cycle sequence). Results are compared for (a) standard Monte Carlo simulations and (b) the FMC calculations described in this paper, for the first three and the last three 100-cycle averages (Fig.2). The FMC results are seen to converge almost immediately and to remain stable in all 100-cycle averages of the run. The FMC data points fluctuate by less than $1\%$ of the maximum amplitude throughout the entire series of 100-cycle-average plots. The reason for the rapid and nearly noiseless convergence of the FMC solution is that the nonlinear functionals depend only weakly on the estimated energy-integrated flux.

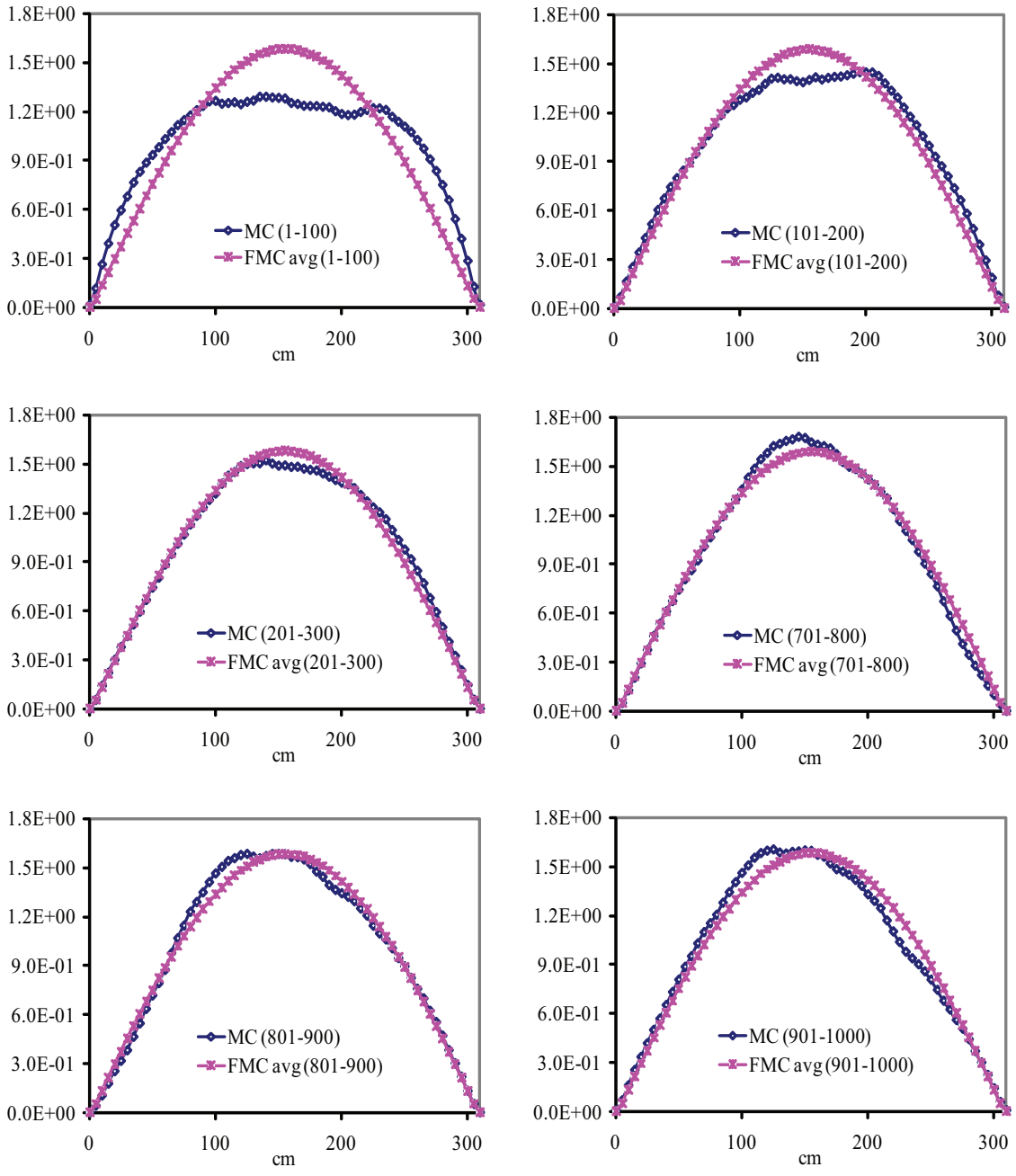


**Figure 2. Problem 1 Energy-Integrated Flux Estimates**

The standard Monte Carlo results converge slowly over the first three 100-cycle averages. However, the Monte Carlo results are also seen to "wobble" away from a cosine shape in the last three averages, showing that true equilibrium is not achieved during the 1000 cycle test run used here. This phenomenon is due to undersampling; it could be suppressed at the cost of greatly increasing the number of Monte Carlo neutrons per cycle.

The estimated values of $k$, with their estimated standard deviations over 10 different ranges of 100 cycles, are given in Table II for the standard Monte Carlo and FMC methods.

**Table II. Estimated $k$ and Standard Deviation for the Homogeneous Fissile Slab Problem**

| Cycles | Standard MC | FMC Average |
|---|---|---|
| 1 to 100 | 0.993737 | 0.995089 |
| | (0.007455) | (0.000003) |
| 101 to 200 | 0.995040 | 0.995088 |
| | (0.005731) | (0.000003) |
| 201 to 300 | 0.995538 | 0.995088 |
| | (0.005254) | (0.000003) |
| 301 to 400 | 0.995097 | 0.995089 |
| | (0.005937) | (0.000003) |
| 401 to 500 | 0.995722 | 0.995088 |
| | (0.005215) | (0.000003) |
| 501 to 600 | 0.995283 | 0.995088 |
| | (0.005367) | (0.000003) |
| 601 to 700 | 0.995493 | 0.995089 |
| | (0.006179) | (0.000003) |
| 701 to 800 | 0.995520 | 0.995088 |
| | (0.005470) | (0.000004) |
| 801 to 900 | 0.995725 | 0.995088 |
| | (0.005827) | (0.000003) |
| 901 to 1000 | 0.995117 | 0.995088 |
| | (0.004933) | (0.000003) |

This table shows that the estimated standard deviations in $k$ obtained with the FMC method are much smaller than the estimated standard deviations in the standard Monte Carlo estimate of $k$. (We do not quantitatively address here the issue that the estimated standard deviation for the Monte Carlo results is smaller than the real standard deviation, due to correlations in the fission source from cycle to cycle. Likewise, we do not address the question of whether the estimates of the FMC standard deviations are accurate. These questions will be addressed in future work. Because the FMC estimates of the eigenfunc-

tion and eigenvalue are so much more stable than the standard Monte Carlo estimates, it is likely that the estimates of the FMC standard deviation are accurate.)

### 2.2.2. Numerical results for two slightly different fissile regions separated by a thick moderator

The coefficients from Eqs. (28) used for this case are presented in Table III. In Eqs. (28), the Macro fission cross-section is assumed to be inversely proportional to $\sqrt{E}$. Though the fission cross-section coefficients are only slightly different in two fissile regions, the difference between these two Macro fission cross-sections becomes greater when the neutron energy decreases. This results a strong peak in the more fissile region on the right and only a small bump in the less fissile region on the left.

**Table III. Cross Section Coefficients for Two Slightly Different Fissile Regions Separated by a Thick Moderator Problem**

| Region | Location | $\Sigma_{s0}(x)$ | $\Sigma_{s1}(x)$ | $\Sigma_{\gamma}(x)$ | $\Sigma_{f}(x)$ |
|---|---|---|---|---|---|
| 1 | $0 < x < 5$ | 0.856 | 0.01 | 0.01 | 0 |
| 2 | $5 < x < 15$ | 0.856 | 0.01 | 0.01 | 0.0089 |
| 3 | $15 < x < 39$ | 0.856 | 0.01 | 0.01 | 0 |
| 4 | $39 < x < 49$ | 0.856 | 0.01 | 0.01 | 0.0090 |
| 5 | $49 < x < 54$ | 0.856 | 0.01 | 0.01 | 0 |

This problem was run for 1000 cycles, using 100,000 histories/cycle. The FMC calculation employed a grid with $h = 0.5$ cm. The estimated energy-integrated flux, averaged over 100-cycle intervals, are compared in Figure 3. Results are compared for (a) standard Monte Carlo simulations and (b) the FMC calculations over cycles 1 to 100, 201 to 300, 401 to 500, 501 to 600, 601 to 700, and 901 to 1000. The FMC results are seen to converge almost immediately and to remain stable in all 100-cycle averages of the run, a result similar to the homogeneous fissile slab case.

The Monte Carlo estimate of the energy-integrated flux seems to converge, but at a very slow pace. The Monte Carlo energy-integrated flux seems to be converged during cycle 601 to 700. In such a case of conventional Monte Carlo simulation, it is necessary to skip the first 600 inactive cycles in order to achieve equilibrium. The standard Monte Carlo simulation would have to skip about 500 times as many particles or cycles as were used in the FMC calculation in order to achieve comparable equilibrium. If we further observe the energy-integrated flux over cycles 901 to 1000 presented in Figure 3, the Monte Carlo energy-integrated flux begins to drift away. There are more fission source particles in the more fissile region on the right, and fewer fission source particles in the less fissile region on the left.

It should also be mentioned that (1), if we run the Monte Carlo simulation long enough, there will be very few or no fission particles left in the less fissile region. This

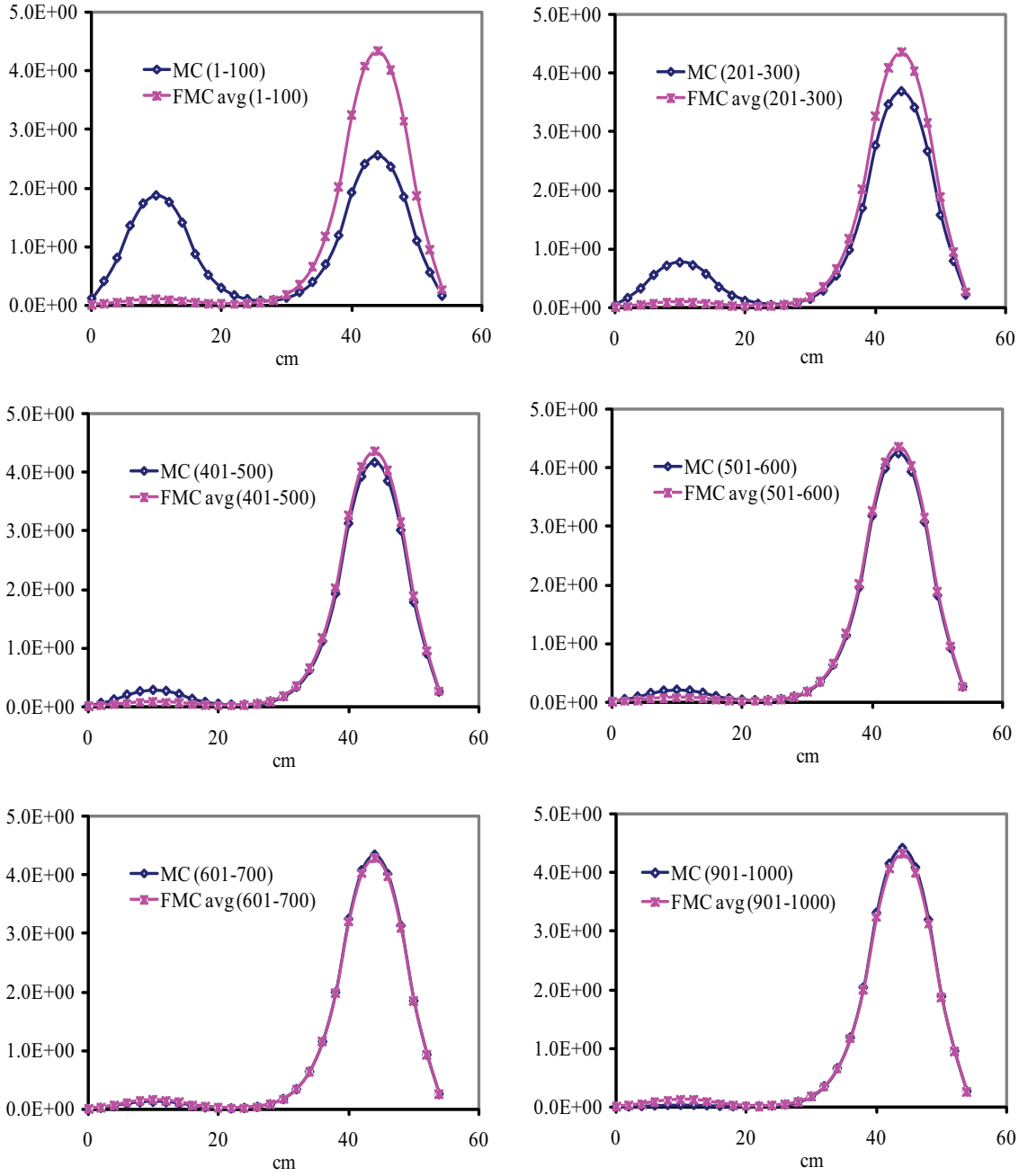


**Figure 3. Problem 2 Energy-Integrated Flux Estimates**

will result in an incorrect spatial shape of the estimated energy-integrated flux. As a consequence, the functionals in Eqs. (26) will not be evaluated correctly. (2) if we have two identical, separated fissile regions, FMC estimates of the energy-integrated flux can vary significantly from one cycle to the next. This occurs for the same reason we described in reference [2], namely the system is very sensitive to small perturbations, and the number

of Monte Carlo particles must be increased to avoid undersampling of the fission source.

The estimated values of $k$, with their estimated standard deviations over 10 different ranges of 100 cycles, are given in Table IV for the standard Monte Carlo method and the FMC method. As before, the FMC $k$-eigenvalue estimates are significantly more accurate than the standard Monte Carlo estimate of $k$.

**Table IV. Estimated $k$ and Standard Deviation for Two Slightly Different Fissile Regions Separated by a Thick Moderator Problem**

| Cycles | Standard MC | FMC Average |
|---|---|---|
| 1 to 100 | 0.777498 | 0.782078 |
| | (0.03522) | (0.00229) |
| 101 to 200 | 0.783256 | 0.781975 |
| | (0.00321) | (0.00049) |
| 201 to 300 | 0.783144 | 0.781867 |
| | (0.00342) | (0.00044) |
| 301 to 400 | 0.783346 | 0.781868 |
| | (0.00350) | (0.00040) |
| 401 to 500 | 0.783673 | 0.781870 |
| | (0.00384) | (0.00044) |
| 501 to 600 | 0.783773 | 0.781921 |
| | (0.00344) | (0.00043) |
| 601 to 700 | 0.784011 | 0.781967 |
| | (0.00352) | (0.00054) |
| 701 to 800 | 0.784707 | 0.781939 |
| | (0.00383) | (0.00042) |
| 801 to 900 | 0.783852 | 0.781940 |
| | (0.00379) | (0.00047) |
| 901 to 1000 | 0.785121 | 0.781883 |
| | (0.00372) | (0.00049) |

We note from Table II that the standard deviations in the FMC estimates of $k$ are more than three orders of magnitude smaller than the Standard MC estimates for the first homogeneous problem, and from Table IV that the standard deviations in the FMC estimates of $k$ are about one order of magnitude smaller than the Standard MC estimates for

the second heterogeneous problem. At this point, it is not completely evident to us why the FMC method performs so much "better" in the first problem than in the second. A possible explanation is that in the work presented here, the nonlinear functionals were evaluated using Monte Carlo data obtained from the Standard Monte Carlo simulations – in which the fission source is never fully converged. If instead, the nonlinear functionals were calculated using Monte Carlo simulations based on the FMC-estimated fission source, we would expect the resulting estimates of $k$ to be much more accurate. We plan to investigate this in future work. We also note that, as with the first problem, the estimated standard deviations for the standard Monte Carlo estimates of $k$ are smaller than the true standard deviations because of the correlations in the fission source from one cycle to the next.

## 3. CONCLUSIONS

The functional Monte Carlo (FMC) hybrid method for solving $k$-eigenvalue problem has been formulated and tested for problems with continuous energy variation of relevant cross-sections. The energy-integrated nonlinear functionals are estimated using standard Monte Carlo techniques with continuous energy. These functionals are then used in an energy-independent low-order equation to estimate the eigenvalue and the energy-integrated flux.

The $k$-eigenvalue and the energy-integrated flux have been evaluated using (a) the FMC method and (b) the standard Monte Carlo method for two simple planar geometries.

In the case of a uniform slab bounded by reflectors, after a sequence of 1000 cycles, each of 50,000 histories, the energy-integrated flux did not achieve equilibrium in the standard Monte Carlo simulation. On the other hand, the FMC-determined energy-integrated flux converged within the first 100 cycles and remained stable throughout. The standard deviation of the estimated k-values was three orders of magnitude smaller for the FMC results than for the standard Monte Carlo estimates.

In the case of two slightly different fissile regions separated by a thick moderator, again, the FMC method converged within the first 100 cycles (100,000 histories/cycle), with a large source distribution peak on the more fissile side, and only a small bump on the less fissile side. The Monte Carlo result appeared to be converged at cycles 601 to 700, then began to drift away at the end of the run. It should be noted that if the Monte Carlo simulation runs long enough, the Monte Carlo source distribution will behave as though there were only one fissile region present. The resulting incorrect spatial shape of the Monte Carlo source distribution will lead to incorrect nonlinear functionals which underpin the FMC calculations.

In future work, we plan to extend the FMC method to 3-D problems with a more realistic continuous energy library. Also, we plan to use the FMC estimate of the fission source distribution as input for the next generation of the Monte Carlo simulation in what would be an iterative scheme, and to examine the question of whether the estimates of the FMC standard deviations in $k$ are more accurate than the standard Monte Carlo estimations.

## ACKNOWLEDGEMENTS

We gratefully acknowledge support of this research through the U. S. Department of Energy NEER grant DE-FG07-04-ID14608 and the University of Michigan Rackham Barbour scholarship.

## REFERENCES

[1] E.W. Larsen and J. Yang, "New 'Monte Carlo Functional' Methods for Evaluating $k$-Eigenvalues and Eigenfunctions," *Trans. Am. Nucl. Soc.,* **97**, 469 (2007).

[2] E.W. Larsen and J. Yang, "A Functional Monte Carlo Method for $k$-Eigenvalue Problems," *Nucl. Sci. Eng.,* **159**, pp.107-126 (2008).

[3] V. YA. GOL'DIN, "A Quasi-Diffusion Method for Solving the Kinetic Equation," *ZH. Vych. Mat.,* **4**, 1078 (1964); English translation published in *USSR Comput. Math. and Math. Phys.,* **4**, 6, 136 (1967).